Supporting Information

Separation and Collision Cross Section Measurements of Protein Complexes Afforded by a Modular Drift Tube Coupled to an Orbitrap Mass Spectrometer

Sarah N. Sipe,[1] James D. Sanders,[1] Tobias Reinecke,[2] Brian H. Clowers,[2] Jennifer S. Brodbelt[1]*
[1]Department of Chemistry, The University of Texas at Austin, Austin, TX 78712
[2]Department of Chemistry, Washington State University, Pullman, WA 99164

*Correspondence to: jbrodbelt@cm.utexas.edu

Contents

Instrumentation details of the modular, ambient drift tube

The drift tube was constructed from printed circuit boards totaling ~20 cm and was assembled as previously described.[1–3] Two, three-grid ion shutters were used to gate ions in and out of the drift region with stopping voltages of 65 V and 80 V, respectively. The design of this home-built drift tube is similar in size and function to a commercially available modular drift tube,[4] which does not currently support FT-IMS multiplexing approaches without instrument modification. Using a 3D-printed adapter, the drift tube was coupled to a prototype Thermo Scientific Q Exactive Plus UHMR Orbitrap mass spectrometer (Bremen, Germany) modified to allow UVPD in the HCD cell as described previously.[5] In-house pulled capillaries coated with a AuPd target were filled with 1-3 µL of each sample and place at the entrance to the PCB-DT using a nano-electrospray ionization (nESI) source. A schematic representation of the instrument is shown in **Figure S1a** of the Supporting Information.

The drift and ESI potentials were controlled using two XP Glassman High Voltage power supplies (High Bridge, NJ). A potential of 10 kV was applied to the entrance of drift tube for a gradient of ~455 V/cm at ambient pressure (~0.6 Townsends). An ESI voltage between 10.7 and 11.1 kV were used for all experiments, corresponding to effect ESI potentials of 0.7 – 1.1 kV. The gates were electrically isolated using pulsers from GAA Custom Engineering (Benton City, WA) and operated simultaneously, controlled using custom LabVIEW program (National Instruments, Austin, TX).[1,3] The parameters of the square-wave frequency sweep (**Figure S2a**) for the FT-IMS experiments of each sample were determined individually and are displayed in **Table S1**. Temperature was recorded using a Neoteck Indoor Outdoor Thermometer and ambient pressure measurements for Austin, TX were obtained from the National Weather Service (w1.weather.gov). Nitrogen was used as the drift gas and was applied at ~1.5 L/min at the exit of the drift tube (entrance to the mass spectrometer).

Arrival time distributions from drift tube IMS can be directly converted to CCS values based on first principles calculations. The reduced mobility (K_0) of each of the ions was determined using equation (1) from the length of the drift tube (l), drift voltage (U), pressure (P), and temperature (T). The Mason-Schamp equation (2) was employed to derive the collision cross section (CCS) from the mobility, mass (μ), and charge (z) of the extracted ions. The remaining variables are constants, including standard temperature, pressure, and buffer gas number density (T_0, P_0, and N_0, respectively), Boltzman's constant (k_b), and elementary charge (e).

$$K_0 = \frac{l^2}{U * t_d} \frac{P}{P_0} \frac{T_0}{T} \quad (1)$$

$$\mathrm{CCS} = \frac{3ze}{16N_0} \left(\frac{2\pi}{\mu k_b T}\right)^{1/2} \frac{1}{K_0} \quad (2)$$

Table S1. Experimental aFT-IMS parameters for each protein in this study.

	Fixed Injection Time (ms)	Start Frequency (Hz)	End Frequency (Hz)	Sweep Duration (min)
Azurin	400	5	7000	10
Calmodulin	400	5	5000	8
Hemoglobin	400	5	5000	8
Streptavidin	200	5	7000	8
Transferrin	300	5	5000	8
Benralizumab	200	5	5000	8

Table S2. The peak CCS values and full width at half maximum are listed for all proteins analyzed in this study organized in ascending order by mass. Experimental CCS values are in good agreement with literature reports.

Protein	Mass (kDa)	Charge State	Literature CCS_{N2} (nm^2)	Experimental $^{DT}CCS_{N2}$ (nm^2)	Full Width at Half Max (nm^2)
azurin monomer	14.0	5	-	15.3	0.5
		6	-	15.7	0.6
		7	-	16.5	0.7
azurin dimer	28.0	8	-	23.7	0.9
		9	-	24.0	0.7
		10	-	24.6	0.4
apo-calmodulin monomer	16.7	6	14.8[6]*	17.0	0.6
holo-calmodulin monomer	16.9	6	15.2[6]*	17.2	0.7
hemoglobin holo-heterodimer	32.3	9	-	27.2	1.5
		10	25.4[7]	27.8	1.2
		11	27.8[7], 29.3[8]	28.4	1.3
hemoglobin holo-heterotetramer	64.7	14	-	42.0	1.2
		15	42.3[7]	42.4	1.0
		16	42.5[7], 43.2[8]	42.9	1.0
apo-streptavidin tetramer	51.9	12	37.7[9]**	37.2	1.5
		13	38.4[9]	37.6	1.1
		14	38.7[9]	38.3	1.1
holo-streptavidin tetramer	52.9	12	-	37.6	1.2
		13	-	38.0	1.0
		14	-	38.4	1.0
apo-transferrin monomer	76.7	15	-	49.3	2.7
		16	-	50.0	2.1
		17	46.32[10]*	50.5	1.7
holo-transferrin monomer	79.8	15	-	49.3	1.8
		16	-	49.7	1.5
		17	45.96[10]*	50.4	1.4
Benralizumab	148.5	20	-	71.4	2.9
		21	72.23[11]***	72.0	2.8
		22	72.25[11]***	72.6	2.6

* Literature CCS values were measured using helium drift gas resulting in smaller CCSs relative to those obtained using nitrogen drift gas.

** Literature CCS values obtained from charge-reducing MS conditions.

*** Literature CCS values are reported for a NIST IgG antibody with similar mass and structure to Benralizumab.

Table S3. aFT-IMS processing parameters for each protein using the first one or three minutes of each sweep acquired using experimental parameters in **Table S1**. The start frequencies and ion injection times were unchanged.

	End frequency (Hz)	
	1-min sweep	**3-min sweep**
Azurin	700	2100
Calmodulin	625	1875
Hemoglobin	625	1875
Streptavidin	875	2625
Transferrin	625	1875
Benralizumab	625	1875

References

(1) Sanders, J. D.; Butalewicz, J. P.; Clowers, B. H.; Brodbelt, J. S. Absorption Mode Fourier Transform Ion Mobility Mass Spectrometry Multiplexing Combined with Half-Window Apodization Windows Improves Resolution and Shortens Acquisition Times. *Anal. Chem.* **2021**, *93* (27), 9513–9520. https://doi.org/10.1021/acs.analchem.1c01427.

(2) Reinecke, T.; Clowers, B. H. Implementation of a Flexible, Open-Source Platform for Ion Mobility Spectrometry. *HardwareX* **2018**, *4*, e00030. https://doi.org/10.1016/j.ohx.2018.e00030.

(3) Sanders, J. D.; Shields, S. W.; Escobar, E. E.; Lanzillotti, M. B.; Butalewicz, J. P.; James, V. K.; Blevins, M. S.; Sipe, S. N.; Brodbelt, J. S. Enhanced Ion Mobility Separation and Characterization of Isomeric Phosphatidylcholines Using Absorption Mode Fourier Transform Multiplexing and Ultraviolet Photodissociation Mass Spectrometry. *Anal. Chem.* **2022**, *94* (10), 4252–4259. https://doi.org/10.1021/acs.analchem.1c04711.

(4) Keelor, J. D.; Zambrzycki, S.; Li, A.; Clowers, B. H.; Fernández, F. M. Atmospheric Pressure Drift Tube Ion Mobility–Orbitrap Mass Spectrometry: Initial Performance Characterization. *Anal. Chem.* **2017**, *89* (21), 11301–11309. https://doi.org/10.1021/acs.analchem.7b01866.

(5) Mehaffey, M. R.; Sanders, J. D.; Holden, D. D.; Nilsson, C. L.; Brodbelt, J. S. Multistage Ultraviolet Photodissociation Mass Spectrometry To Characterize Single Amino Acid Variants of Human Mitochondrial BCAT2. *Anal. Chem.* **2018**, *90* (16), 9904–9911. https://doi.org/10.1021/acs.analchem.8b02099.

(6) Wyttenbach, T.; Grabenauer, M.; Thalassinos, K.; Scrivens, J. H.; Bowers, M. T. The Effect of Calcium Ions and Peptide Ligands on the Relative Stabilities of the Calmodulin Dumbbell and Compact Structures. *J. Phys. Chem. B* **2010**, *114* (1), 437–447. https://doi.org/10.1021/jp906242m.

(7) Scarff, C. A.; Patel, V. J.; Thalassinos, K.; Scrivens, J. H. Probing Hemoglobin Structure by Means of Traveling-Wave Ion Mobility Mass Spectrometry. *J Am Soc Mass Spectrom* **2009**, *20* (4), 625–631. https://doi.org/10.1016/j.jasms.2008.11.023.

(8) Woodall, D. W.; Brown, C. J.; Raab, S. A.; El-Baba, T. J.; Laganowsky, A.; Russell, D. H.; Clemmer, D. E. Melting of Hemoglobin in Native Solutions as Measured by IMS-MS. *Anal. Chem.* **2020**, *92* (4), 3440–3446. https://doi.org/10.1021/acs.analchem.9b05561.

(9) Stiving, A. Q.; Jones, B. J.; Ujma, J.; Giles, K.; Wysocki, V. H. Collision Cross Sections of Charge-Reduced Proteins and Protein Complexes: A Database for Collision Cross Section Calibration. *Anal. Chem.* **2020**, *92* (6), 4475–4483. https://doi.org/10.1021/acs.analchem.9b05519.

(10) Booyjžsen, C.; Scarff, C. A.; Moreton, B.; Portman, I.; Scrivens, J. H.; Costantini, G.; Sadler, P. J. Fibrillation of Transferrin. *Biochimica et Biophysica Acta (BBA) - General Subjects* **2012**, *1820* (3), 427–436. https://doi.org/10.1016/j.bbagen.2011.11.004.

(11) Campuzano, I. D. G.; Larriba, C.; Bagal, D.; Schnier, P. D. Ion Mobility and Mass Spectrometry Measurements of the Humanized IgGk NIST Monoclonal Antibody. In *State-of-the-Art and Emerging Technologies for Therapeutic Monoclonal Antibody Characterization Volume 3. Defining the Next Generation of Analytical and Biophysical Techniques*; Schiel, J. E., Davis, D. L., Borisov, O. V., Eds.; American Chemical Society, Series Ed.; ACS Symposium Series; American Chemical Society: Washington, DC, 2015; Vol. 1202, pp 75–112. https://doi.org/10.1021/bk-2015-1202.ch004.

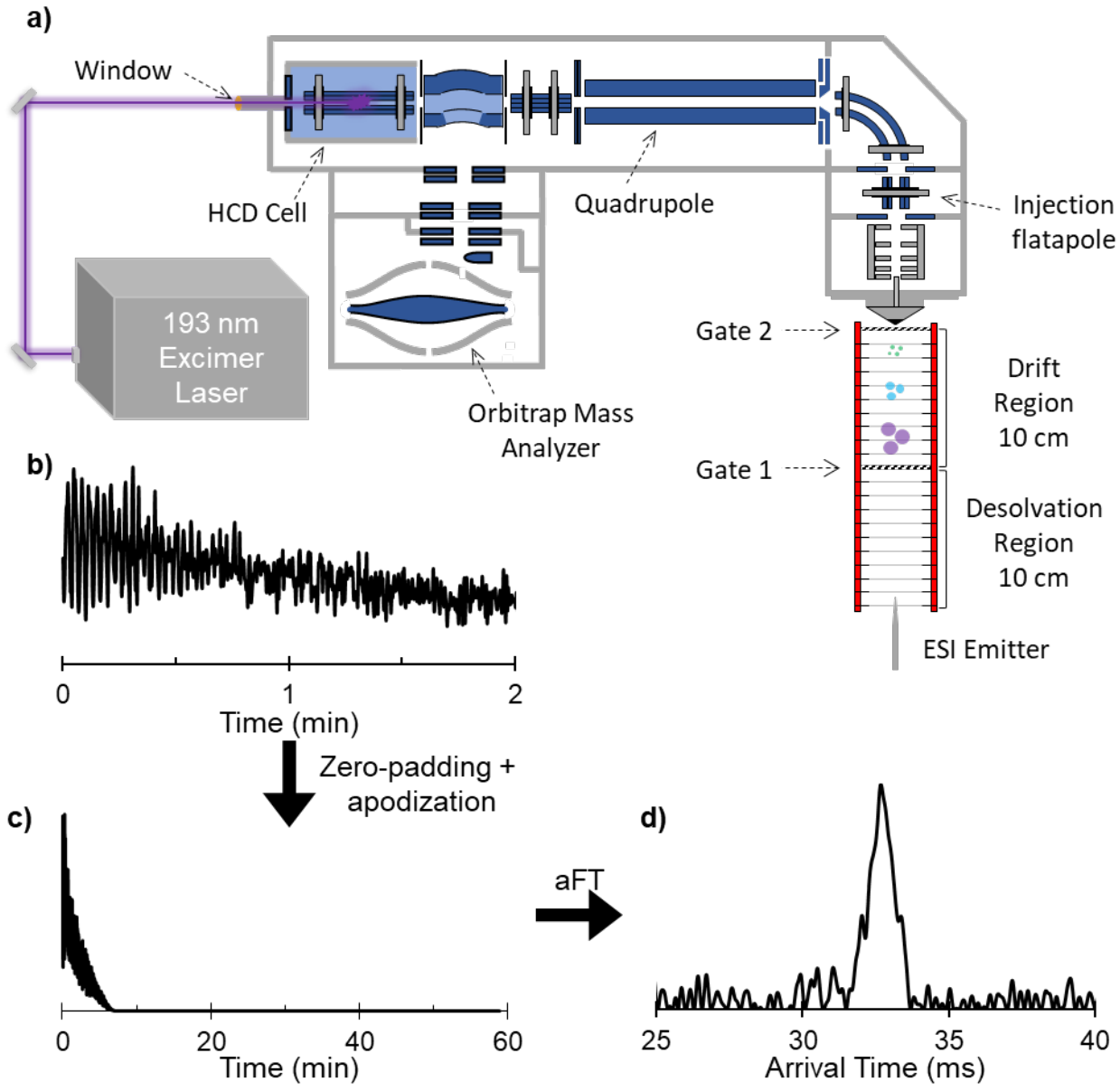

Figure S1. a) Instrument schematic of the ~20 cm drift tube affixed to the front-end of an Ultra High Mass Range Orbitrap mass spectrometer, equipped with in-source trapping for desolvation, followed by UVPD in the HCD cell prior to mass analysis. b) Extracted ion chromatogram of an ion during an 8-minute FT-IMS sweep zoomed to the first two minutes. Ion frequency can be seen in the first minute before diminishing signal. c) Zero-padding and half-window apodization performed prior to d) transformation with absorption mode FT resulting in an arrival time distribution.

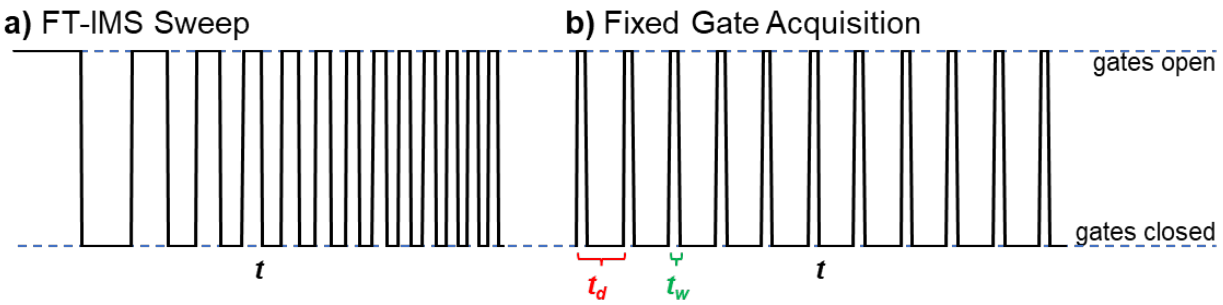

Figure S2. The pulsing scheme for the dual-gate drift tube. Both gates are operated synchronously, opened and closed using a square waveform with a) a frequency swept from low to high for FT-IMS experiments or b) a frequency fixed to a desired drift time (t_d) with a designated pulse width (t_w).

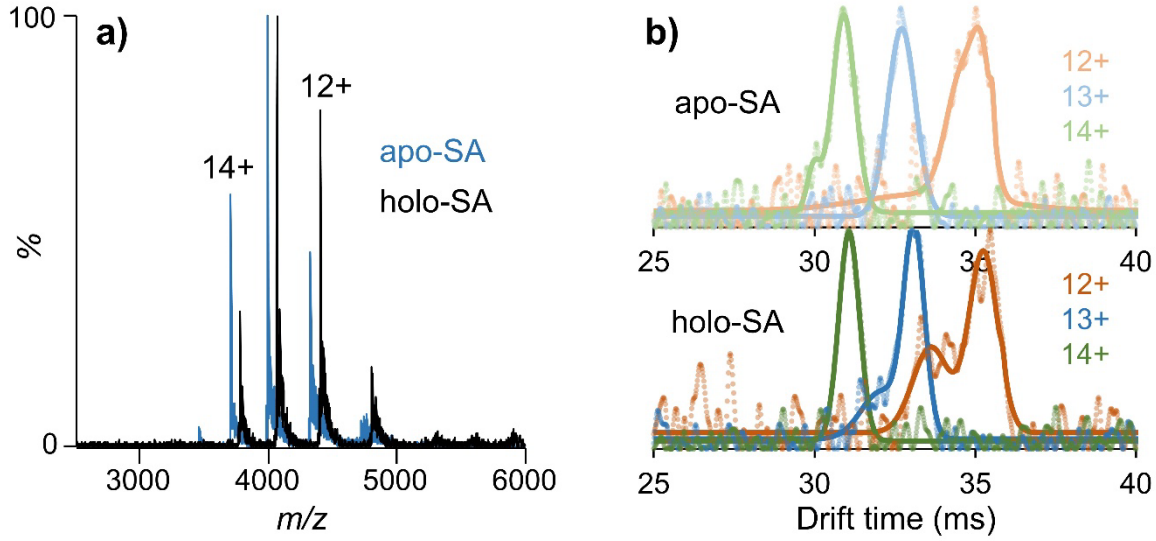

Figure S3. a) Overlaid nESI mass spectra of apo- (blue) and holo-streptavidin (black) using the PCB-IMS with both gates open. b) ATDs of apo- and holo-streptavidin tetramers (12+ through 14+) produced from transformation of averaged extracted ion chromatograms generated during 8-min aFT-IMS sweeps. The raw data are represented as circles and the fitted data are overlaid as solid lines.

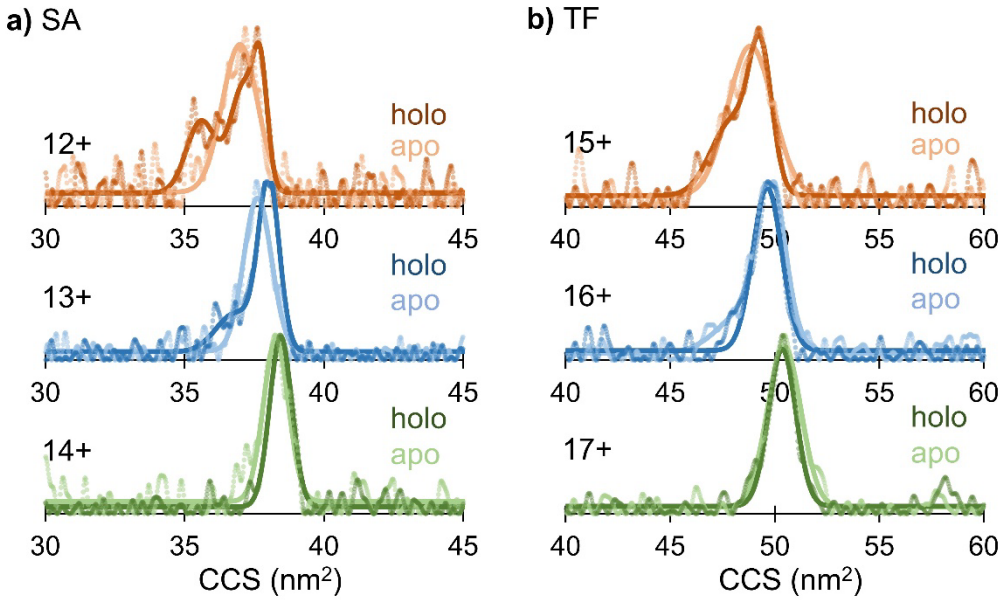

Figure S4. Overlaid collision cross section distributions of a) streptavidin tetramers and b) transferrin monomers bound (holo) or unbound (apo) to their ligands, biotin and Fe(III), respectively, following 8-min aFT-IMS sweeps. The raw data are represented as circles and the fitted data are overlaid as solid lines.

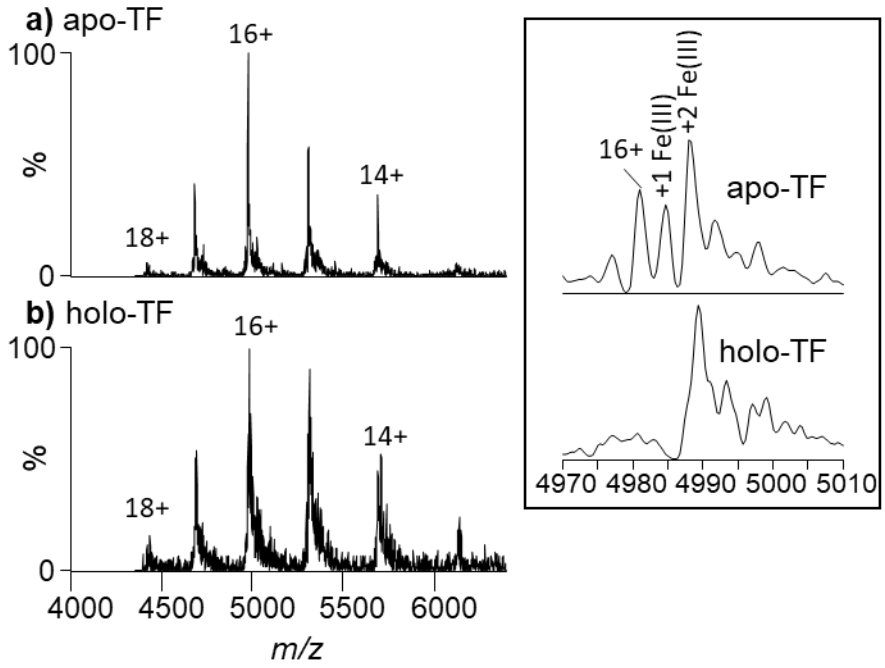

Figure S5. Representative nESI mass spectra of a) apo-transferrin and b) holo-transferrin using the PCB-IMS with both gates open. Inset shows expansion of the 16+ charge states of apo- and holo-TF demonstrating resolution of iron-bound states.

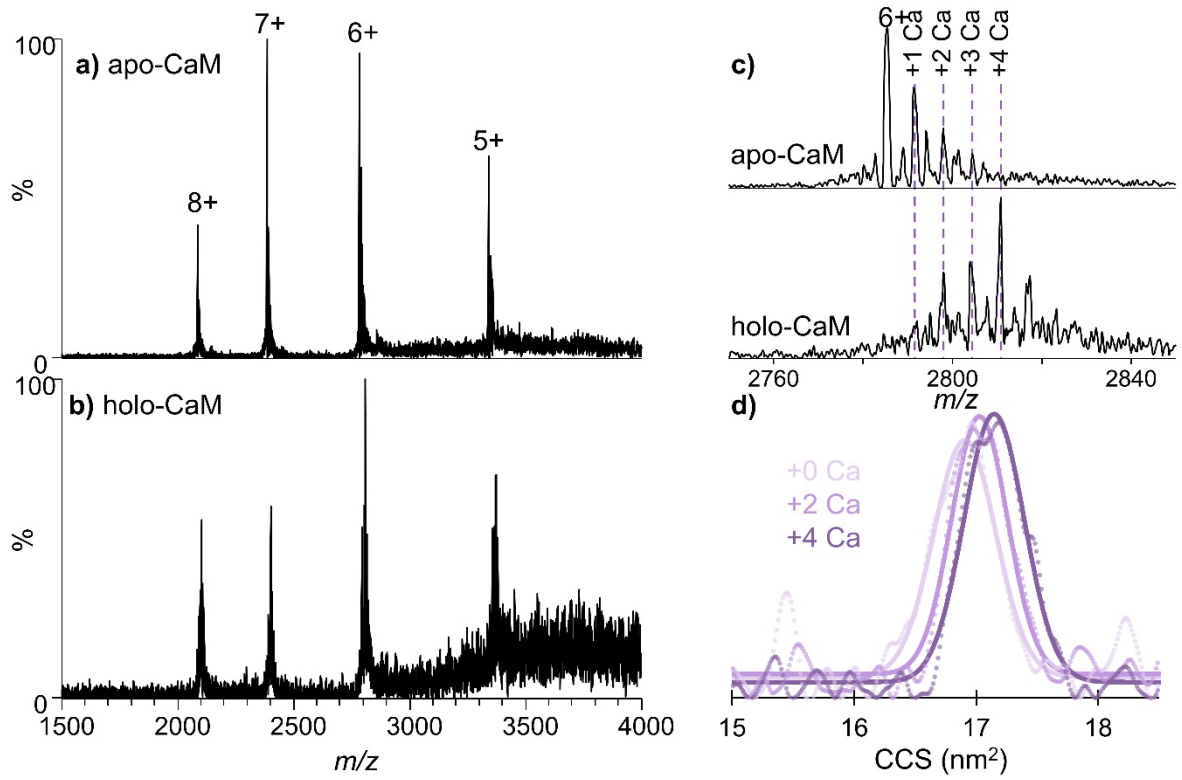

Figure S6. Representative nESI mass spectra of a) apo-calmodulin and b) holo-calmodulin obtained using the PCB-IMS. c) Magnification of 6+ charge state demonstrating resolution of Ca-bound states. d) CCS distributions of apo (0 Ca) and holo (2 and 4 Ca bound) calmodulin obtained following 8-min aFT-IMS sweeps with the raw data represented as circles and the fitted data overlaid as lines. CCS distributions of calmodulin containing 1 or 3 Ca are omitted to minimize congestion of the figure.

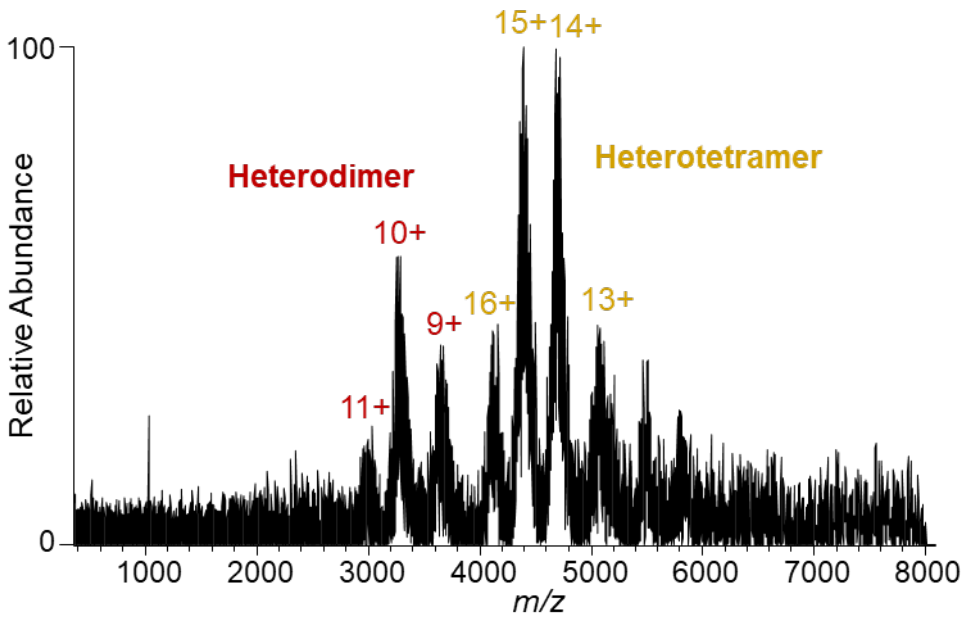

Figure S7. Representative nESI mass spectra of hemoglobin obtained using the PCB drift tube with both gates open. No desolvation energy was applied to avoid disassembly of protein complexes.

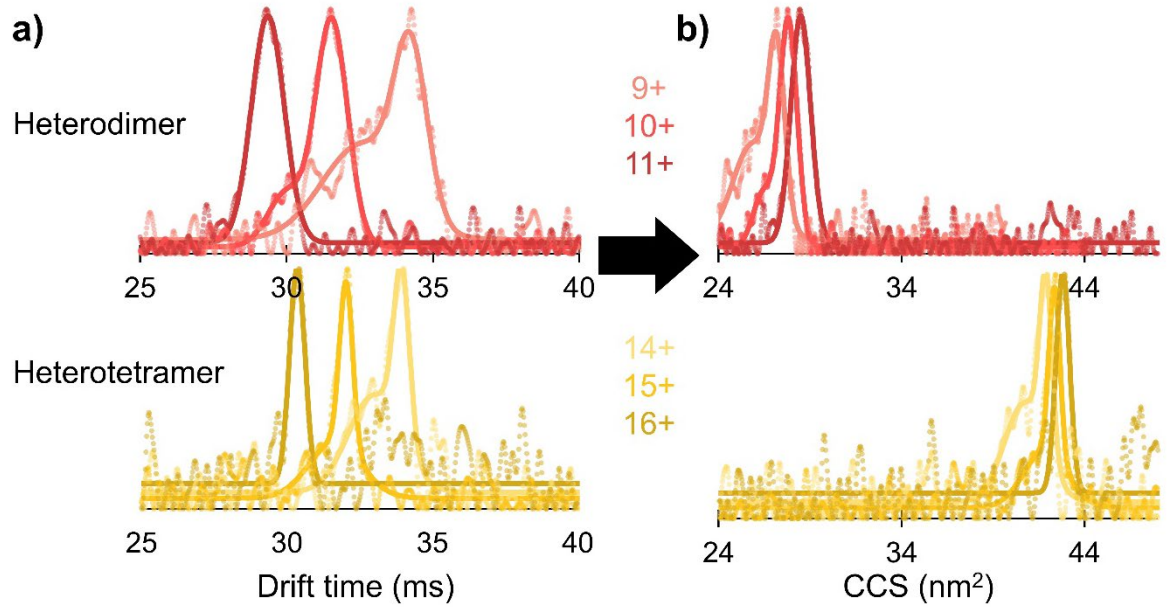

Figure S8. a) ATDs of holo-hemoglobin heterodimers and heterotetramers converted to b) collisional cross section distributions following 8-min aFT-IMS sweeps. The raw data are represented as circles and the fitted data are overlaid as solid lines.

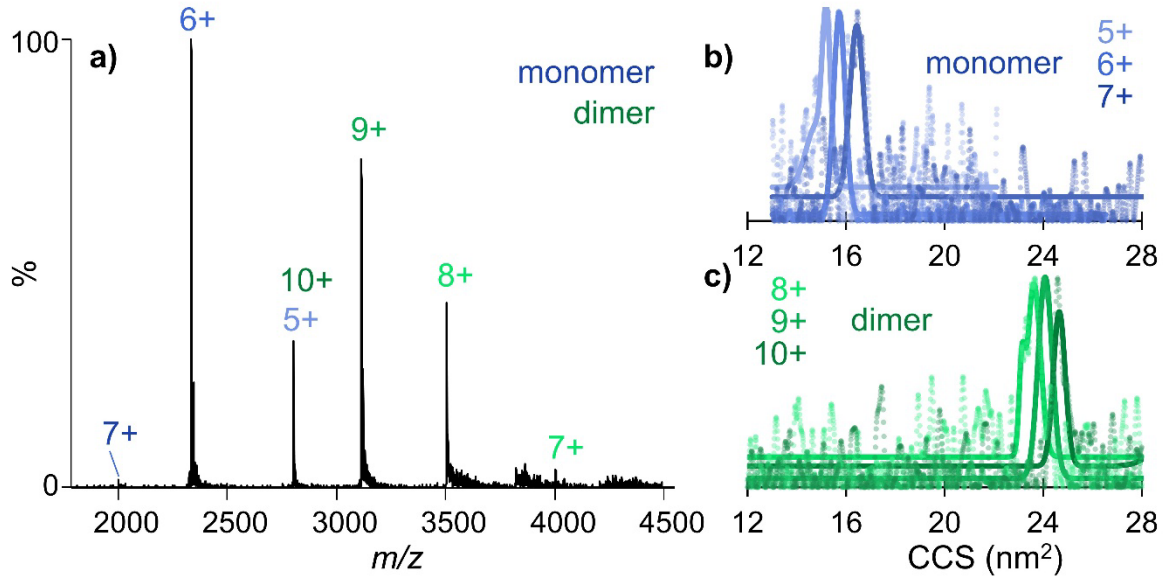

Figure S9. a) Representative nESI mass spectra of azurin generated using the PCB-IMS. CCS distributions of b) Az monomers and c) Az dimers following a 10-min aFT-IMS sweep with raw data represented as circles and the fitted data overlaid as solid lines.

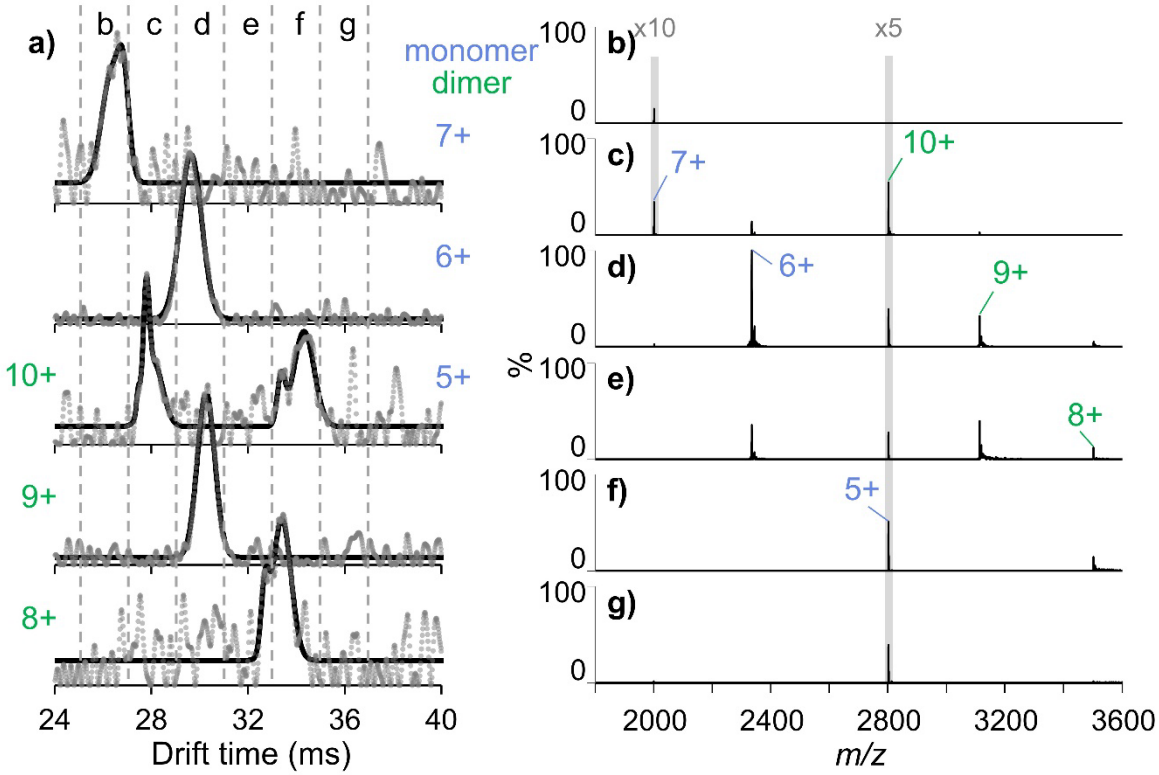

Figure S10. a) ATDs obtained from 10-min aFT-IMS sweeps of azurin with raw data represented as circles and the fitted data overlaid as solid lines. Mass spectra obtained using fixed gate acquisition from b) 25-27 ms, c) 27-29 ms, d) 29-31 ms, e) 31-33 ms, f) 33-35 ms, and g) 35-37 ms corresponding to the periods demarcated by dashed lines in (a). Ions at *m/z* 2002 and 2802 are magnified for visibility.

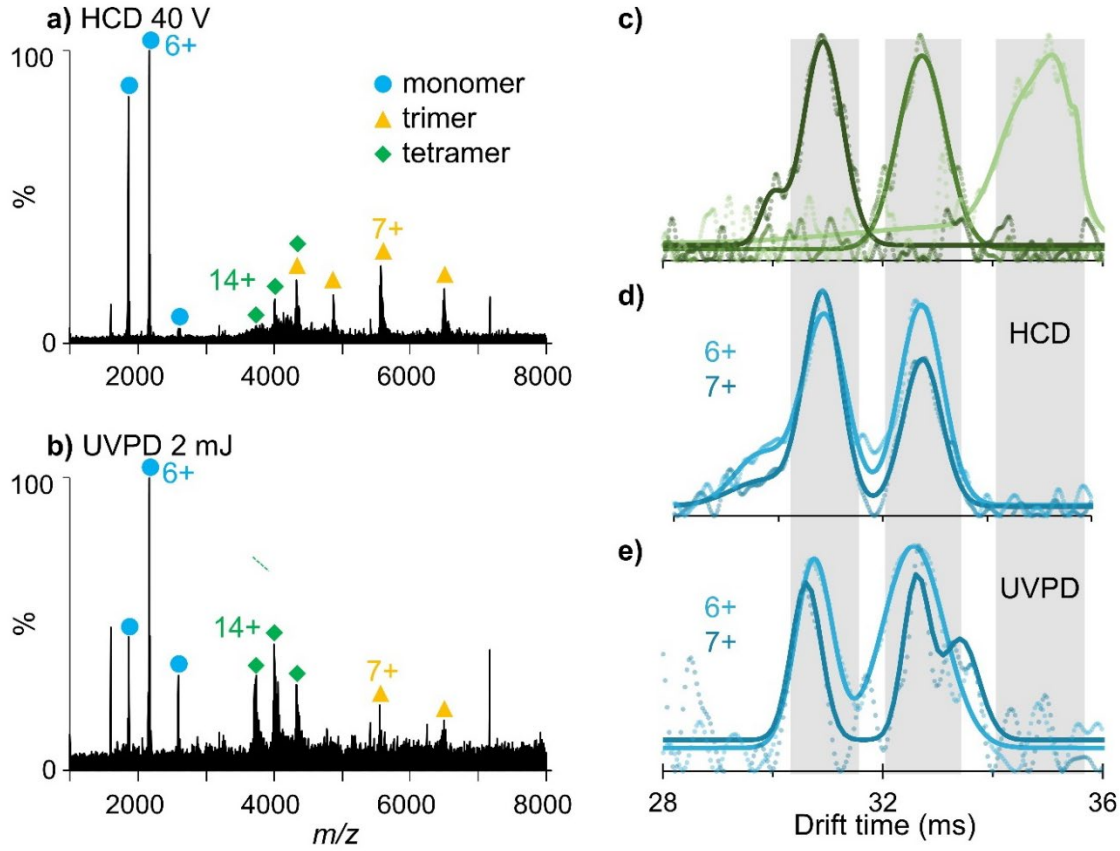

Figure S11. Representative MS/MS spectra of streptavidin tetramers (12+ through 14+) subjected to a) 40 V HCD and b) 1 pulse, 2 mJ UVPD. c) ATDs of tetrameric streptavidin obtained from 8-min aFT-IMS sweeps. Frequency-tagged monomers resulting from d) HCD and from e) UVPD obtained from 20-min aFT-IMS sweeps. The raw data for all ATDs are represented as circles and the fitted data are overlaid as solid lines. Drift times of ejected monomers correspond to the tetrameric precursors from which they were generated.

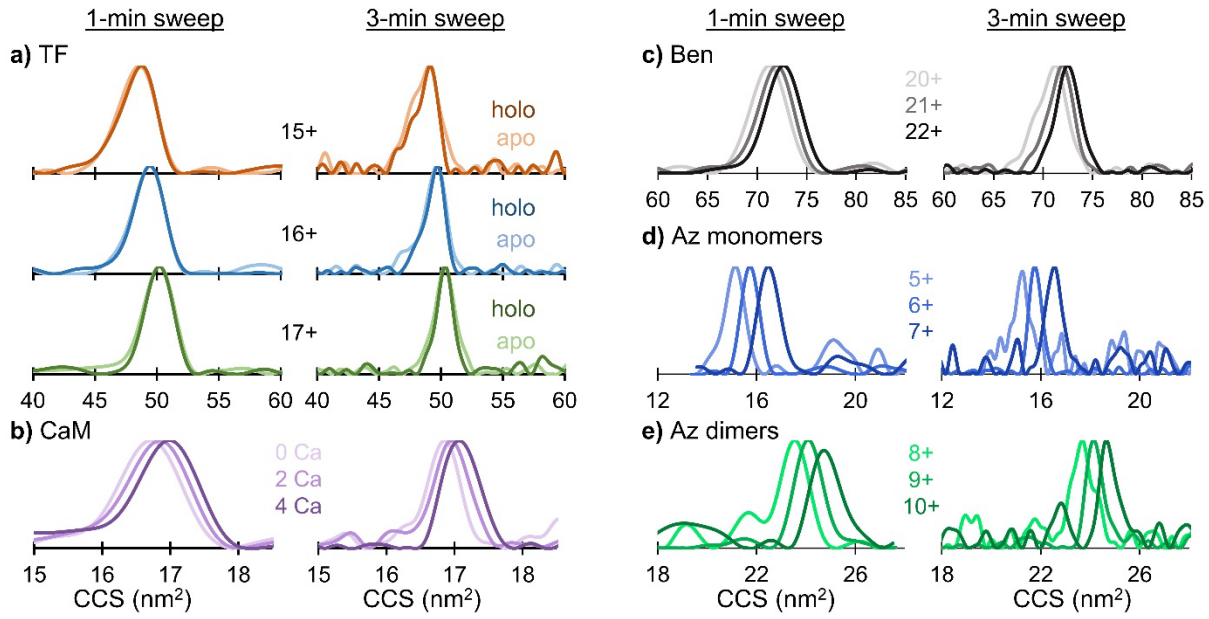

Figure S12. CCS distributions for a) apo- and holo-transferrin, b) apo- and holo-calmodulin, c) benralizumab, d) azurin monomers, and e) azurin homodimers using truncated FT-IMS acquisition times.